sustainability

MDPI

Article

Activation of Persulfate by Sulfide-Modified Nanoscale Zero-Valent Iron Supported on Biochar for 2,4-Dichlorophenol Degradation: Efficiency, Sustainability, and Mechanism Investigation

Mu Wang [1,2,3], Yan Zhao [1], Zongsheng An [1] and Changming Dou [1,*]

[1] Anhui Provincial Academy of Eco-Environmental Science Research, Hefei 230026, China; wangmucjl@163.com (M.W.); yanzhao.ahhky@gmail.com (Y.Z.); anzongsheng100@sina.com (Z.A.)
[2] College of Civil and Hydraulic Engineering, Bengbu University, Bengbu 233030, China
[3] School of Earth and Space Sciences, University of Science and Technology of China, Hefei 230026, China
* Correspondence: doucm@sina.com

Abstract

The activation of persulfate (PS) to oxidize and degrade 2,4-dichlorophenol (2,4-DCP) in aqueous solution represents a prevalent advanced oxidation technology. This study established a PS activation system using sulfide-modified nanoscale zero-valent iron supported on biochar (S-nZVI@BC). The optimal conditions included a PS:2,4-DCP mass ratio of 70:1 and S-nZVI@BC:PS of 1.5:1. The activator had excellent stability after being reused five times, which lead to high cost-effectiveness and sustainable usability. This system exhibited broad pH adaptability (3–11), with enhanced efficiency under acidic/neutral conditions. Chloride ion, nitrate, and carbonate had effects during the degradation. During the initial degradation phase, S-nZVI@BC played a primary role, with a greater contribution rate of adsorption than reduction. Fe^0 played a dominant role in the PS activation process; reactive species—including HO•, SO_4•$^-$, and O_2•$^-$—were identified as key agents in subsequent degradation stages. The overall degradation processes comprised three distinct stages: dechlorination, ring-opening, and mineralization.

Keywords: 2,4-dichlorophenol; sulfide modification; nanoscale zero-valent iron; persulfate; sustainable usability

check for updates

Academic Editor: Giovanni De Feo

Received: 21 August 2025
Revised: 15 September 2025
Accepted: 25 September 2025
Published: 28 September 2025

Citation: Wang, M.; Zhao, Y.; An, Z.; Dou, C. Activation of Persulfate by Sulfide-Modified Nanoscale Zero-Valent Iron Supported on Biochar for 2,4-Dichlorophenol Degradation: Efficiency, Sustainability, and Mechanism Investigation. *Sustainability* **2025**, *17*, 8721. https://doi.org/10.3390/su17198721

Copyright: © 2025 by the authors. Licensee MDPI, Basel, Switzerland. This article is an open access article distributed under the terms and conditions of the Creative Commons Attribution (CC BY) license (https://creativecommons.org/licenses/by/4.0/).

1. Introduction

Chlorophenols (CPs) are a class of chlorinated aromatic compounds composed of benzene rings, hydroxyl groups, and chlorine atoms. Owing to their antibacterial properties and unique reactivity, CPs have found extensive application in agricultural and industrial sectors [1,2]. However, their high chemical stability and resistance to biodegradation lead to persistence in the natural environment, rendering them significant and widespread environmental pollutants [3]. Especially, 2,4-dichlorophenol (2,4-DCP) is a common persistent pollutant detected in agricultural production, chlorination-disinfected water, and paper mill wastewater [4,5]. Conventional methods for CPs' removal include adsorption, membrane separation, and biodegradation [6]. Nevertheless, these approaches exhibit limitations: adsorbents, upon saturation, require incineration or disposal, posing risks as secondary pollution sources [7]; membrane separation proves inefficient for treating wastewater with high CP concentrations; and the biodegradation processing cycle is long [1].

Advanced oxidation processes (AOPs) currently represent more effective technologies for treating toxic organic pollutants [8]. They utilize catalytic methods—such as light, ultra-

sound, electricity, and catalysts—to activate various oxidants, generating active substances with high redox potential. These enable the efficient degradation, even mineralization of recalcitrant organic pollutants. Common oxidants incorporate ozone (O_3), hydrogen peroxide (H_2O_2), and persulfate (PS) [8–10]. Among them, the PS-based advanced oxidation process (PS-AOP) has garnered significant attention in recent years [11]. The PS oxidation technology was proposed after experimental verification [12]. During the electrolysis process, sulfate can generate PS, which has oxidizing ability. Compared to O_3 and H_2O_2, PS offers distinct advantages: a wider variety of activation modes [13], simultaneously producing multiple reactive oxygen species (ROS) during the activation process, including sulfate radical ($SO_4\bullet^-$), hydroxyl radical (HO•), and superoxide radical ($O_2\bullet^-$) [14], higher free radical yields [15], lower dependence on environmental conditions [16], and existing in solid state makes it more conducive for storage and transportation [17].

PS has certain oxidation ability, but the degradation efficiency is relatively low. Generally, it needs to be activated through different methods for generating more active substances with higher redox potential [18]. Iron-based materials have been extensively investigated as activators for PS due to their environmentally friendly nature, relative low toxicity, and cost-effectiveness [19,20]. However, nZVI exhibits low efficiency as a kind of PS activator, primarily attributed to particle aggregation, surface passivation, and inefficient electron transfer [21]. To address these deficiencies, various nZVI modification techniques have been explored. Among them, biochar (BC) loading and sulfide modification have been proven particularly effective [21–24].

BC is the thermal decomposition product of waste biomass under the anoxic condition and is a stable compound rich in carbon [25]. The BC-supported nZVI composite has gained significant attention owing to its high contaminant adsorption capacity, good electrical conductivity, and enhanced nZVI reactivity. The properties and preparation conditions of BC (such as pore structure, functional group, raw material composition, and pyrolysis temperature) are of crucial importance in determining the properties of BC-supported nZVI [21,22].

On the other hand, sulfide-modified iron-based materials are easy to prepare. Depending on the form of sulfur, sulfur-iron compounds such as FeS, Fe_3S_4, FeS_2, and Fe_9S_{11} can be obtained. Among them, FeS is more common [26]. Sulfide modification enhances the hydrophobicity and salt resistance of nZVI, reduces electron transfer resistance to contaminants, blocks atomic hydrogen adsorption sites, and inhibits the water reduction reaction and consequent H_2 evolution [23,24].

Despite possessing these advantages, research concerning activation methods and reaction mechanisms in combination utilizing sulfide-modified and BC-supported iron-based materials remains relatively scarce. For instance, Chen et al. [27] demonstrated the feasibility and mechanism of S-nZVI@BC for trichloroethylene (TCE) removal in groundwater remediation, and their results indicated that S-nZVI@BC, synergistically combining the high adsorption capacity of BC with the strong reductive capacity of S-nZVI, outperformed either component alone. Similarly, Xie et al. [28] synthesized S-nZVI@BC and specifically investigated the influencing factors with activation mechanisms involved in the PS degradation of 2-chlorophenol; they found that S-nZVI@BC had excellent stability and sustainability, could be reused multiple times, and was worthy of in-depth research.

When using degradable materials for pollutants, it is very important to conduct an analysis regarding their environmental friendliness and sustainability. Kayode et al. [29] employed a life-cycle assessment (LCA) to evaluate the environmental impact of coupling hydrothermal carbonization (HTC) with anaerobic digestion (AD) compared to conventional AD treatment. HTC degraded wastewater sludge in an aqueous medium, producing carbon-dense hydrochar while reducing sludge volumes. Elif et al. [30] presented a foun-

dational overview of LCA principles and described a systematic, step-by-step procedure for its effective application. Additionally, this article revisited the fundamental concepts of carbon footprint (CF) analysis as a complementary tool for quantifying greenhouse gas emissions associated with products and activities.

In this study, S-nZVI@BC composites were synthesized using different composition ratios. The effects of key operational parameters on degradation efficiency were systematically investigated by using the method of controlling variables, including the following: the mass ratio of PS:2,4-DCP and S-nZVI@BC:PS, initial pH, reaction temperature, and the concentrations of specific background ions. Component contribution analysis quantified the adsorption and reduction in S-nZVI@BC according to the 2,4-DCP removal rate at the initial stage of the reaction. Furthermore, the degradation mechanism and the relative contributions of various reactive species were elucidated using oxidant scavenger experiments and electron spin resonance (ESR) spectroscopy.

2. Materials and Methods

2.1. Chemicals and Reagents

All chemical reagents were of analytical grade or higher and used as received without further purification. Iron nitrate nonahydrate ($Fe(NO_3)_3 \bullet 9H_2O \geq 98.5\%$), sodium sulfide ($Na_2S \bullet 9H_2O \geq 98.5\%$), 1,10-phenanthroline ($C_{12}H_8N_2 \bullet H_2O \geq 98.0\%$), and tert-butyl alcohol (TBA, $C_4H_{10}O \geq 98.0\%$) were supplied by Sinopharm Chemical Reagent Co., Ltd. (Shanghai, China). Sodium persulfate (PS, $Na_2S_2O_8 \geq 99.0\%$), 2,4-dichlorophenol (2,4-DCP, $C_6H_4Cl_2O \geq 99.0\%$), potassium borohydride (PBH, $KBH_4 \geq 99.0\%$), 5, 5-Dimethyl-1-pyrroline-N-oxide (DMPO, $C_6H_{11}NO \geq 99.0\%$), iron sulfate heptahydrate ($FeSO_4 \bullet 7H_2O \geq 99.0\%$), and p-benzoquinone (BQ, $C_6H_4O_2 \geq 99.0\%$) were obtained from Shanghai Macklin Biochemical Co., Ltd. (Shanghai, China). Hydrochloric acid (HCl, 36.0–38.0%), sulfuric acid (H_2SO_4 95.0%–98.0%), sodium hydroxide ($NaOH \geq 99.0\%$), sodium chloride ($NaCl \geq 99.5\%$), sodium carbonate ($Na_2CO_3 \geq 99.5\%$), and sodium nitrate ($NaNO_3 \geq 99.5\%$) were sourced from Tianjin Kermel Chemical Reagent Co., Ltd. (Tianjin, China). Methanol (MeOH, $CH_4O \geq 99.9\%$) was a guaranteed reagent provided by Shanghai Weston Trading Co., Ltd. (Shanghai, China). Rice husk was purchased from a green plant base in Hefei, China. The ultrapure water used throughout the experiments was produced by a Synergy UV water purification system (Merck Millipore, Grenoble, France).

2.2. Synthesis of S-nZVI@BC

The synthesis of S-nZVI@BC included BC preparation, a reaction in the liquid phase to obtain nZVI and sulfide-modification. Rice husk was chosen as the material for preparing BC as a common agricultural waste. It was collected and dried under 105 °C in the air-dry oven for 24 h before being used. The dried material was then placed in an OTF-1200X type tube-heating furnace. The pyrolysis process was carried out under a constant nitrogen purge. The temperature was first ramped from ambient to 600 °C at a rate of 10 °C/min, held at 600 °C for 2 h, and dropped to room temperature in four hours. The final BC product was ground into a powder and sieved (50-mesh) for subsequent use.

S-nZVI@BC was synthesized in a two-step method. Quantitative BC was added to a quantitative $Fe(NO_3)_3$ solution of 200 mL, stirring constantly for 30 min with constant nitrogen purge, and then the suspension was subsequently treated by the dropwise addition of 200 mL KBH_4 solution under stirring. After 10 min of reaction, 110 mL of Na_2S solution was introduced, followed by 30 min of ultrasonication. The resulting solid product was then collected by filtration and thoroughly washed with ultrapure water until the filtrate conductivity fell below 50 μS/cm. Lastly, the material was dried in a freeze dryer (the temperature was set to −50 °C) and the S-nZVI@BC was obtained after 24 h. The mass

ratio of PBH and $Fe(NO_3)_3 \bullet 9H_2O$ was 1.3:1 when preparing the reaction reagents, and the additive amounts of BC, $Fe(NO_3)_3 \bullet 9H_2O$, and $Na_2S \bullet 9H_2O$ were regulated to make the mass ratio of Fe to C approximately 1:2 and S to Fe approximately 1:4, respectively.

2.3. Experimental Processes

All reactions were conducted in 500 mL flasks containing 400 mL of 2,4-DCP solution. S-nZVI@BC and PS were added at specified dosages, with the total volume adjusted to 500 mL using ultrapure water. The degradation experiments were conducted in a thermostatic reciprocating shaker (SHA-B, Shanghai, China) at 180 rpm and set temperatures (10, 30, and 50 °C). Liquid samples were withdrawn at predetermined time intervals (10, 30 min, 1, 2, 4, 8, 16, 24, 48, 72 h) and immediately filtered through 0.22 mm membranes. Then, 0.5 mL of solution was transferred into the special sample vial and capped for determination after adding 0.5 mL MeOH to stop the reaction.

The material of BC was rice husk, while the pyrolysis temperature value was 600 °C, the mass ratio of S:Fe:C = 1:4:8, and the initial 2,4-DCP concentration was 20 mg/L. A series of batch experiments were conducted to determine the optimal reaction conditions and evaluate the influence of key parameters. The investigated variables and their ranges were as follows: the mass ratio of PS to 2,4-DCP (0, 10, 20, 30, 40, 50, 60, 70, and 80), the mass ratio of S-nZVI@BC to PS (0, 0.2, 0.4, 0.6, 0.8, 1.0, 1.2, 1.5, and 2.0), the initial pH (3.0, 5.0, 7.0, 9.0, and 11.0), the reaction temperature (10 °C, 30 °C, and 50 °C), and the concentration of background anions (chloride ion, nitrate ion, carbonate ion; 0, 50, 100, 200, and 500 mg/L). All experiments were performed in duplicate, and the reported data represent the average of the measurements, and were analyzed mainly by Excel 2016 and Origin 2021.

Component contribution analysis was applied to analyze the actions of adsorption and reduction according to the mass ratio of BC, S-nZVI, and nZVI in the S-nZVI@BC. Four ingredients were added to the 2,4-DCP solution with 20 mg/L of 400 mL, which were S-nZVI@BC 0.84 g, BC 0.517 g, S-nZVI 0.177 g, and nZVI 0.146 g (the dosages of ingredients were calculated by the mass ratio of S:Fe:C = 1:4:8, and FeS was regarded as the main component of S-nZVI). The actions of adsorption reduction were quantified by determinating the degradation of 2,4-DCP at predetermined time intervals of 10, 30 min, 1, 2, 4, 8, 16, 24, 48, 72 h. Then, to desorb the 2,4-DCP from the ingredients, the pH of the solution was adjusted to 12 by adding 1 mM NaOH. After 5 min of violent shaking, 2,4-DCP was measured in the solution after immediate filtration, and the difference value before and after desorption could be used to quantify the adsorption capacity of materials [31].

2.4. Analytical Methods

The concentration of 2,4-DCP was determined by high performance liquid chromatograph (HPLC) (Thermo Scientific U3000, Thermo Scientific, Waltham, MA, USA) with the Athena C18-WP column (250 mm × 4.6 mm, 5 μm). The following operating conditions were employed: column temperature of 40 °C, detection wavelength of 254 nm, a mobile phase ratio of V(water):V(MeOH) = 3:7, a flow rate of 1.0 mL/min, and a sample injection volume of 10 μL. The pH and conductivity of aqueous solutions were measured using a PHBJ-260 portable pH meter and a DDS-307 conductivity meter, respectively.

The physicochemical properties of S-nZVI@BC before and after reactions were characterized as follows. The Brunauer–Emmett–Teller (BET) surface areas were measured by N_2 adsorption using a speci-tellfic surface area and mesoporous distribution analyzer (Micromeritics Tristar II 3020, Micromeritics, Atlanta, GA, USA). The surface features used a scanning electron microscope (SEM) with Energy Disperse Spectroscopy (EDS) (GeminiSEM 500, ZEISS, Oberkochen, Germany). X-ray photoelectron spectroscopy (XPS) data were obtained with an X-ray photoelectron spectrometer (Thermo Scientific ESCALAB 250Xi,

Thermo Scientific, Waltham, MA, USA). X-ray diffraction (XRD) analysis was conducted with a multifunctional rotating target X-ray diffractometer (Rigaku SmartLab, Tokyo, Japan). The functional group analysis was obtained with a fourier transform infrared spectrometer (FTIR) (Nicolet 8700, Thermo Scientific, Waltham, MA, USA).

Electron spin resonance (ESR) spectroscopy (JES-FA200, JEOL Ltd., Tokyo, Japan) was employed to identify reactive oxygen species (HO•, SO_4•$^-$ and O_2•$^-$) generated in the reaction systems. ESR measurements were conducted at the University of Science and Technology of China under the following conditions: temperature maintained at 25 °C using a circulating water system, a microwave frequency set at 9.84 GHz (X-band), and 5,5-dimethyl-1-pyrroline-N-oxide (DMPO) used as the spin-trapping agent. HO• and SO_4•$^-$ were detected in pure water solution, and O_2•$^-$ was detected with MeOH reagent (v:v = 1:1). Spectrometer parameters were as follows: a microwave frequency of 8.75–9.65 GHz (X-band), central magnetic field of 3245.0 G, microwave energy of 2 mW, modulation frequency of 100 kHz, scanning width of 50 G, time constant of 0.03 s, and scanning frequency of once every 30 s.

3. Results and Discussion

3.1. Characterization of Prepared Materials

The basic structures of BC, S-nZVI, and S-nZVI@BC before and after reaction were analyzed using SEM, the element compositions of them were obtained by EDS, and the results are presented in Figure 1a–d and Figure S1, respectively. As shown in Figure 1a, BC exhibited a smooth surface and provided a honeycomb structure for S-nZVI, with carbon and oxygen being the predominant elements (Figure S1a). Figure 1b reveals that S-nZVI possessed a flocculent agglomeration structure with numerous pores, primarily composed of iron, oxygen, carbon, and sulfur (Figure S1b). Figure 1c demonstrates that S-nZVI nanoparticles were densely packed onto the BC surface, nearly covering it completely. Compared to BC, the increased proportions of iron and sulfur elements (Figure S1c) indicate the successfully loading of these elements on the BC surface during S-nZVI@BC preparation. Following the reaction, Figure 1d shows a reappearance of a smooth carbon skeleton on the surface of S-nZVI@BC. This observation, coupled with a reduction in the proportions of iron and sulfur (Figure S1d), suggests the consumption of these elements during the reaction. Collectively, these results demonstrate that BC provided abundant binding sites, effectively mitigating S-nZVI agglomeration, and consequently enhancing the activation of PS by S-nZVI to generate free radicals.

The crystal structures of S-nZVI@BC materials before and after reaction were analyzed by XRD. Figure 1e presents the obtained XRD patterns within the 2θ range of 10° to 80°. The spectra for both fresh and reacted S-nZVI@BC exhibit a diffraction peak at approximately 2θ = 22.5° and 22.6°, respectively, corresponding to the characteristic peak of rice husk BC. A distinct characteristic peak of Fe^0 is observed at 2θ = 44.92° in both spectra, confirming the successful reduction in Fe^{3+} to Fe^0 during material synthesis. Characteristic peaks indicative of FeS are also evident at 2θ = 35.46°(fresh) and 35.32°(reacted), demonstrating the presence of FeS and successfully sulfidation modification of nZVI [32]. Finally, weak diffraction peaks appeared at 2θ = 61.92°(fresh) and 62.12°(reacted), suggesting that an iron oxide protective film was formed on the material surface. This observation is consistent with the increased oxygen content detected in Figure S1c,d.

Functional group analysis of S-nZVI@BC before and after reaction was conducted using FT-IR spectroscopy. Figure 1f displays the obtained spectra within the wavenumber range of 400–4000 cm^{-1}. The most prominent absorption band at ~3412 cm^{-1} corresponds to the O–H stretching vibrations of hydroxyl groups on the BC surface. A distinct band at ~1385 cm^{-1} arises from the stretching vibrations of other BC surface functional groups.

Post-reaction, both bands exhibited reduced intensity relative to fresh S-nZVI@BC, indicating hydroxyl group participation in degradation reactions and possible coverage by precipitated iron hydroxides. The band at ~1627 cm^{-1}, due to C = O stretching in carboxyl groups (–COOH), maintained consistent intensity before and after reaction, suggesting minimal involvement of carboxyl groups in 2,4-DCP degradation. The C–O vibration band at ~1104 cm^{-1} [33] intensified following the reaction, implying increased carbon–oxygen bonding. This likely results from oxygen incorporation and iron leaching during degradation, consistent with EDS elemental analysis. A new band emerged at ~568 cm^{-1} in reacted samples, potentially assignable to either Fe–O vibrations (from surface Fe^0 oxidation) or sulfide-related bonds, confirming successful material sulfidation.

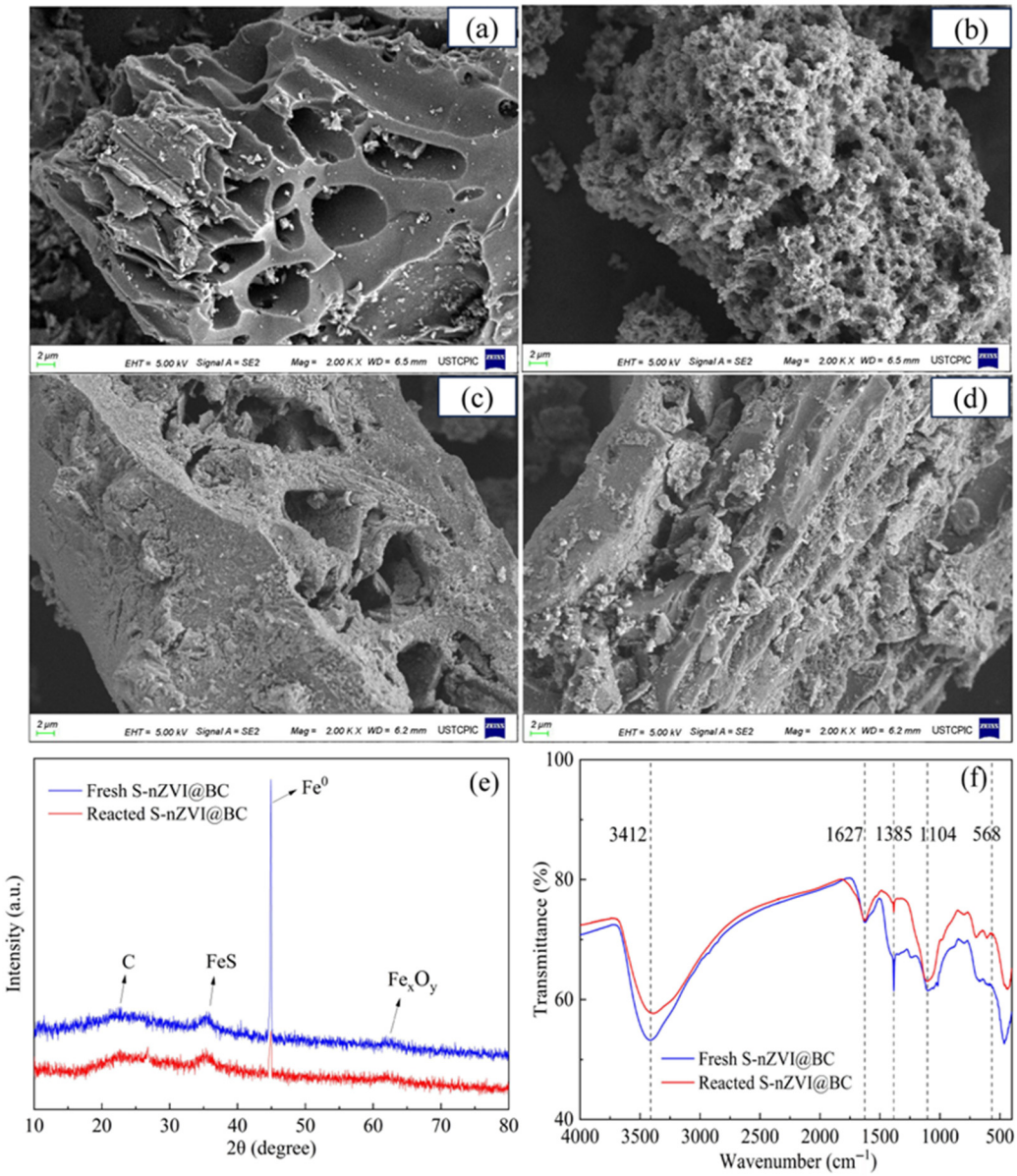


Figure 1. SEM images of (**a**) BC, (**b**) S-nZVI, (**c**) fresh S-nZVI@BC, and (**d**) reacted S-nZVI@BC; the magnifications of the SEM images are all 2.00 k×. (**e**) XRD analysis and (**f**) infrared spectra of fresh S-nZVI@BC and reacted S-nZVI@BC. Reaction condition: PS = 1400 mg/L, [2,4-DCP] = 20 mg/L of 400 mL, BC@S-nZVI = 2100 mg/L, initial pH = 9 ± 0.2, T = 30 °C.

To investigate the adsorption properties of materials through their specific surface area and pore structure characteristics, BET analysis was conducted on dehydrated S-nZVI, BC,

and S-nZVI@BC composites before and after reaction. The results are shown in Table S1. BC exhibited the largest BET surface area (351.76 m^2/g) and total pore volume (0.29 cm^3/g) among all samples. These values exceeded those of pristine S-nZVI, fresh S-nZVI@BC, and reacted S-nZVI@BC. The reduction in both parameters for S-nZVI@BC is attributed to pore blockage by S-nZVI particles during composite formation. Post-reaction, the partial consumption of S-nZVI liberated occupied pore spaces, resulting in an increased surface area and pore volume relative to fresh composite [34].

3.2. Effects of Different Degradation Systems

Determining optimal oxidant and activator dosages constitutes fundamental research in organic pollutant degradation systems [28,35]. The effects of reagent dosage were evaluated by varying the mass ratios of PS to 2,4-DCP and S-nZVI@BC to PS, with the corresponding degradation efficiencies shown in Figure 2a,b. Figure 2a demonstrates the influence of the PS:2,4-DCP mass ratio (where C_t and C_0 represent 2,4-DCP concentrations at time t and initial state, respectively). At a fixed activator concentration, increasing the PS:2,4-DCP ratio from 0 to 70 enhanced 2,4-DCP removal from 10.9% to 97.4% within 72 h. This improvement is attributed to enhanced radical generation via S-nZVI@BC-mediated PS activation (Equations (1)–(6)) [36], where a higher PS dosage promotes oxidative species production. However, further increasing the ratio to 80 reduced the removal efficiency to 91.7%, likely due to radical scavenging through $SO_4\bullet^-$ self-quenching or reaction with excess PS (Equations (7) and (8)). Consequently, a PS:2,4-DCP of 70 was the optimum mass ratio for subsequent experiments.

$$Fe^0 + S_2O_8^{2-} \rightarrow Fe^{2+} + 2SO_4^{2-} \quad (1)$$

$$2Fe^0 + O_2 + 2H_2O \rightarrow 2Fe^{2+} + 4OH^- \quad (2)$$

$$Fe^{2+} + S_2O_8^{2-} \rightarrow Fe^{3+} + SO_4^{2-} + SO_4\bullet^- \quad (3)$$

$$Fe^0 + S_2O_8^{2-} + 2H_2O \rightarrow Fe^{2+} + 2HO\bullet + 2SO_4^{2-} + 2H^+ \quad (4)$$

$$Fe^0 + 2S_2O_8^{2-} \rightarrow Fe^{2+} + 2SO_4\bullet^- + 2SO_4^{2-} \quad (5)$$

$$2H_2O + 2S_2O_8^{2-} \rightarrow O_2\bullet^- + 4H^+ + 3SO_4^{2-} + SO_4\bullet^- \quad (6)$$

$$SO_4\bullet^- + SO_4\bullet^- \rightarrow S_2O_8^{2-} \quad (7)$$

$$SO_4\bullet^- + S_2O_8^{2-} \rightarrow SO_4^{2-} + S_2O_8\bullet^- \quad (8)$$

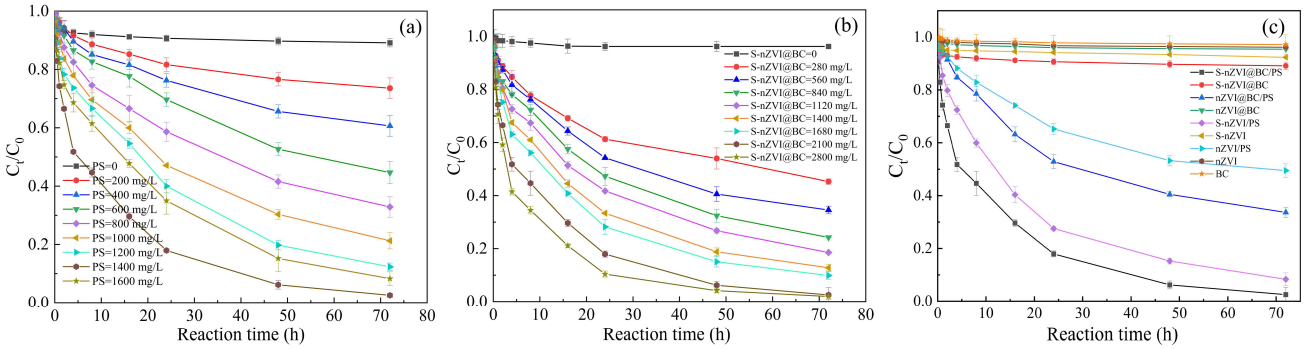


Figure 2. Effect of different activation systems on the degradation of 2,4-DCP: (**a**) different mass concentration of PS with fixed value [S-nZVI@BC] = 2100 mg/L, (**b**) different mass concentration of S-nZVI@BC with fixed value [PS] = 1400 mg/L, (**c**) different reaction systems with mass ratio of PS to 2,4-DCP was 70, S-nZVI@BC, nZVI@BC, S-nZVI, and nZVI to PS were 1.5. Reaction condition: [2,4-DCP] = 20 mg/L of 400 mL, initial pH = 9 ± 0.2, T = 30 °C.

Figure 2b illustrates the mass ratio of S-nZVI@BC:PS's influence on 2,4-DCP degradation. At a fixed PS concentration, increasing the S-nZVI@BC:PS ratio from 0 to 1.5 enhanced 2,4-DCP removal from 3.8% to 97.4% within 72 h. A further increase to 2.0 with the degradation rate only improved slightly (98.0%), indicating that the activation of PS by S-nZVI@BC reached a saturated state. This plateau effect likely results from the excessive Fe^{2+} release at a high activator dosage, which scavenges $SO_4\bullet^-$ via oxidative consumption Equation (9) [28], thereby reducing radical availability for pollutant degradation. Consequently, the optimal S-nZVI@BC:PS mass ratio was determined as 1.5 for subsequent studies.

$$Fe^{2+} + SO_4\bullet^- \rightarrow Fe^{3+} + SO_4^{2-} \quad (9)$$

Figure 2c compares 2,4-DCP degradation efficiencies across nine relevant systems under identical conditions. After 72 h, the removal rates followed the order: S-nZVI@BC/PS (97.4%) > S-nZVI/PS (91.7%) > nZVI@BC/PS (66.3%) > nZVI/PS (50.5%) ≫ S-nZVI@BC (10.9%) ≈ S-nZVI (7.6%) ≈ nZVI@BC (4.6%) ≈ nZVI (3.8%) ≈ BC (2.8%).

Notably, systems lacking PS activation exhibited minimal removal (<11%), while nZVI@BC/PS and nZVI/PS achieved only 50.5–66.3% efficiency. In contrast, both sulfide modification systems (S-nZVI@BC/PS and S-nZVI/PS) demonstrated significantly enhanced degradation, with S-nZVI@BC/PS achieving near-complete pollutant removal (97.4%). These results confirm that sulfide modification and BC support synergistically activate PS, where there is a higher degradation rate after sulfide modification due to the improved nZVI hydrophobicity and electron transfer capacity [27,28]. Consequently, the S-nZVI@BC/PS system represents an efficient PS-based AOP for 2,4-DCP wastewater remediation.

3.3. Effects of Different Influencing Factors

The reusability of S-nZVI@BC in PS activation was evaluated through five consecutive 2,4-DCP degradation cycles (72 h each). Post-reaction, the catalyst underwent triple washing with deionized water/methanol, followed by freeze-drying for reuse. As depicted in Figure 3a, 2,4-DCP removal decreased from 97.4% (cycle 1) to 74.0% (cycle 5), confirming retained catalytic activity after multiple cycles.

Notably, efficiency declined rapidly during initial cycles (cycles 1–3) but stabilized subsequently. This biphasic deactivation pattern is attributed to the following: (i) Irreversible adsorption of degradation intermediates on active sites, persisting despite solvent washing [36]. (ii) Progressive iron precipitation reducing accessible Fe^{2+} species and active component content [37]. Despite these mechanisms, S-nZVI@BC demonstrates robust stability in PS activation for sustained 2,4-DCP degradation.

The energy required for recycling materials was lower than that needed for reproducing, and it also reduced the usage of related raw materials and lead to widespread environmental and economic benefits.

According to the calculation, oxidation degradation one ton 2,4-DCP with concentration of 20 mg/L, the cost of using H_2O_2 is CNY 8640. Not including the equipment cost for preparing O_3, the cost is CNY 2716, and the cost of the S-nZVI@BC/PS system is CNY 4860. The cost of an industrial O_3 generator is approximately several tens of thousands of yuan. Moreover, the preparation of O_3 requires a large amount of electricity. After comprehensive analysis, the S-nZVI@BC/PS system is still more energy-efficient and environmentally friendly.

Under optimized conditions, the key parameters on 2,4-DCP degradation effects are presented in Figure 3b–f. Batch experiments evaluating pH influence (Figure 3b) revealed distinct kinetic patterns: complete removal (100%) occurred at 4 h (pH = 3), 48 h (pH = 5), and 72 h (pH = 7), and efficiency declined to 91.1% at pH = 11.

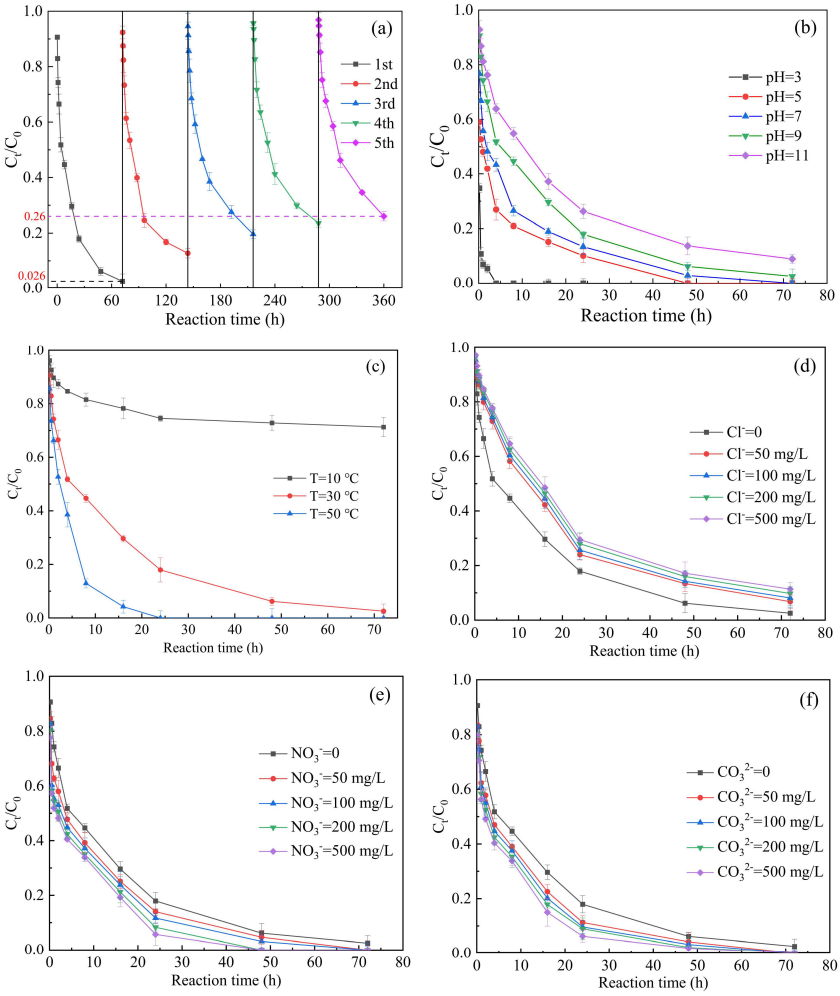


Figure 3. Effect of different influence factors on the degradation of 2,4-DCP (**a**) recycle tests of S-nZVI@BC, (**b**) pH, (**c**) temperature, (**d**) Cl^-, (**e**) NO_3^-, (**f**) CO_3^{2-}. Reaction condition: PS = 1400 mg/L, [2,4-DCP] = 20 mg/L of 400 mL, BC@S-nZVI = 2100 mg/L, initial pH = 9 ± 0.2, T = 30 °C.

This demonstrates effective PS activation by S-nZVI@BC across acidic to neutral pH (3–7), outperforming alkaline conditions. The enhanced degradation effects at a lower pH are attributed to the following: (i) Accelerated $SO_4\bullet^-$ generation via facilitated PS decomposition (Equation (10)). (ii) Reduced activation energy for radical production. (iii) Suppressed formation of passivating iron hydroxide layers. Conversely, alkaline conditions (pH = 11) promote the following: active site occlusion by $Fe(OH)_x$ precipitates, $SO_4\bullet^-$ conversion to less oxidative •OH (E^0 = 1.9–2.7 V vs. 2.5–3.1 V), and Equations (11) and (12) collectively diminishing degradation efficiency [38]. Furthermore, acidic conditions lower the activation energy barrier for PS activation, accelerating radical generation kinetics and thereby enhancing 2,4-DCP degradation efficiency [39].

$$S_2O_8^{2-} + H^+ \rightarrow SO_4\bullet^- + SO_4^{2-} + H^+ \quad (10)$$

$$Fe^{3+} + 3OH^- \rightarrow Fe(OH)_3 \downarrow \quad (11)$$

$$SO_4\bullet^- + OH^- \rightarrow SO_4^{2-} + HO\bullet \quad (12)$$

Figure 3c demonstrates the temperature dependence of 2,4-DCP degradation. A dramatic reduction in removal efficiency occurred with decreasing temperature (50 °C → 10 °C), evidenced by a complete pollutant elimination within 16 h at 50 °C versus merely 23.7% removal

after 72 h at 10 °C. This aligns with the established literature confirming enhanced persulfate activation kinetics and contaminant degradation at elevated temperatures [40].

The influence of anions on 2,4-DCP degradation presented in the S-nZVI@BC/PS system. Chloride ion (Cl^-) exhibited inhibitory effects (Figure 3d), reducing the removal efficiency from 97.4% (no Cl^-) to 88.6% at 500 mg/L within 72 h. This attenuation is attributed to radical scavenging mechanisms: Cl^- carries out a reaction with $SO_4\bullet^-$ to form less reactive chlorine radicals (Cl•, Equation (13)) [41], which exhibit a lower oxidative capacity toward phenolic compounds.

Conversely, both nitrate (NO_3^-) and carbonate (CO_3^{2-}) enhanced degradation kinetics (Figure 3e,f). At 500 mg/L concentration, NO_3^- achieved complete removal (100%) within 48 h (vs. 97.4% control) and CO_3^{2-} reached 100% removal within 72 h. This acceleration aligns with reports [42,43] on secondary radical generation ($NO_3\bullet/CO_3\bullet^-$ via Equations (14) and (15)), which rapidly oxidize phenolic contaminants at elevated concentrations.

$$SO_4\bullet^- + Cl^- \rightarrow SO_4^{2-} + Cl\bullet \quad (13)$$

$$SO_4\bullet^- + NO_3^- \rightarrow SO_4^{2-} + NO_3\bullet \quad (14)$$

$$SO_4\bullet^- + CO_3^{2-} \rightarrow SO_4^{2-} + CO_3\bullet^- \quad (15)$$

3.4. Analysis of XPS

XPS was employed to probe iron speciation and binding energy evolution in S-nZVI@BC before and after degradation (Figure 4). The Fe2p 3/2 high-resolution spectrum of fresh material (Figure 4a) revealed three deconvoluted peaks at 706.1 eV (Fe^0), 710.9 eV [Fe(II)], and 713.3 eV [Fe(III)], confirming the successful reduction in Fe^{3+} to Fe^0 during synthesis.

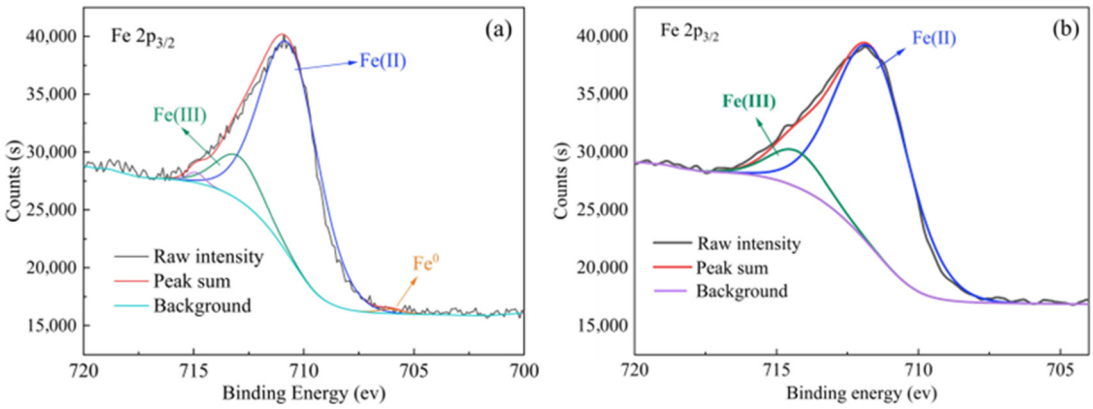


Figure 4. XPS analysis of (**a**) fresh S-nZVI@BC and (**b**) reacted S-nZVI@BC. Reaction condition: PS = 1400 mg/L, [2,4-DCP] = 20 mg/L of 400 mL, BC@S-nZVI = 2100 mg/L, initial pH = 9 ± 0.2, T = 30 °C.

Post-reaction (Figure 4b), the Fe2p 3/2 spectrum exhibited two dominant components at 711.9 eV [Fe(II)] and 714.6 eV [Fe(III)], indicating the surface oxidation and depletion of Fe^0 during 2,4-DCP degradation. Survey spectra (Figure S2) further verified the coexistence of Fe, O, C, and S elements through characteristic Fe 2p, O 1s, C 1s, and S 2p photoelectron peaks [44].

3.5. Degradation Mechanisms Analysis

The mechanisms of S-nZVI@BC on 2,4-DCP includes the adsorption of BC and reductive de-chlorination of S-nZVI and nZVI [27,37]. Component contribution analysis

(Figure 5a) quantified these mechanisms according to the 2,4-DCP removal rate. The sum of BC adsorption, S-nZVI reduction, and nZVI reduction was greater than the actions of S-nZVI@BC, which simultaneously includes adsorption and reduction; it meant that the preparation of the S-nZVI@BC was not a simple mixture of several components, but S-nZVI loaded on the BC as a whole. The reactive sites and pores of BC were filled; therefore, the overall performance of the S-nZVI@BC was lower than the sum of the removal effects of each raw material. Furthermore, the removal rate of S-nZVI@BC on 2,4-DCP increased from 4.5% of 10 min to 10.9% of 72 h, in which the action of adsorption was more dominant than the action of reduction, increasing from 2.9% after 10 min to 7.5% after 72 h.

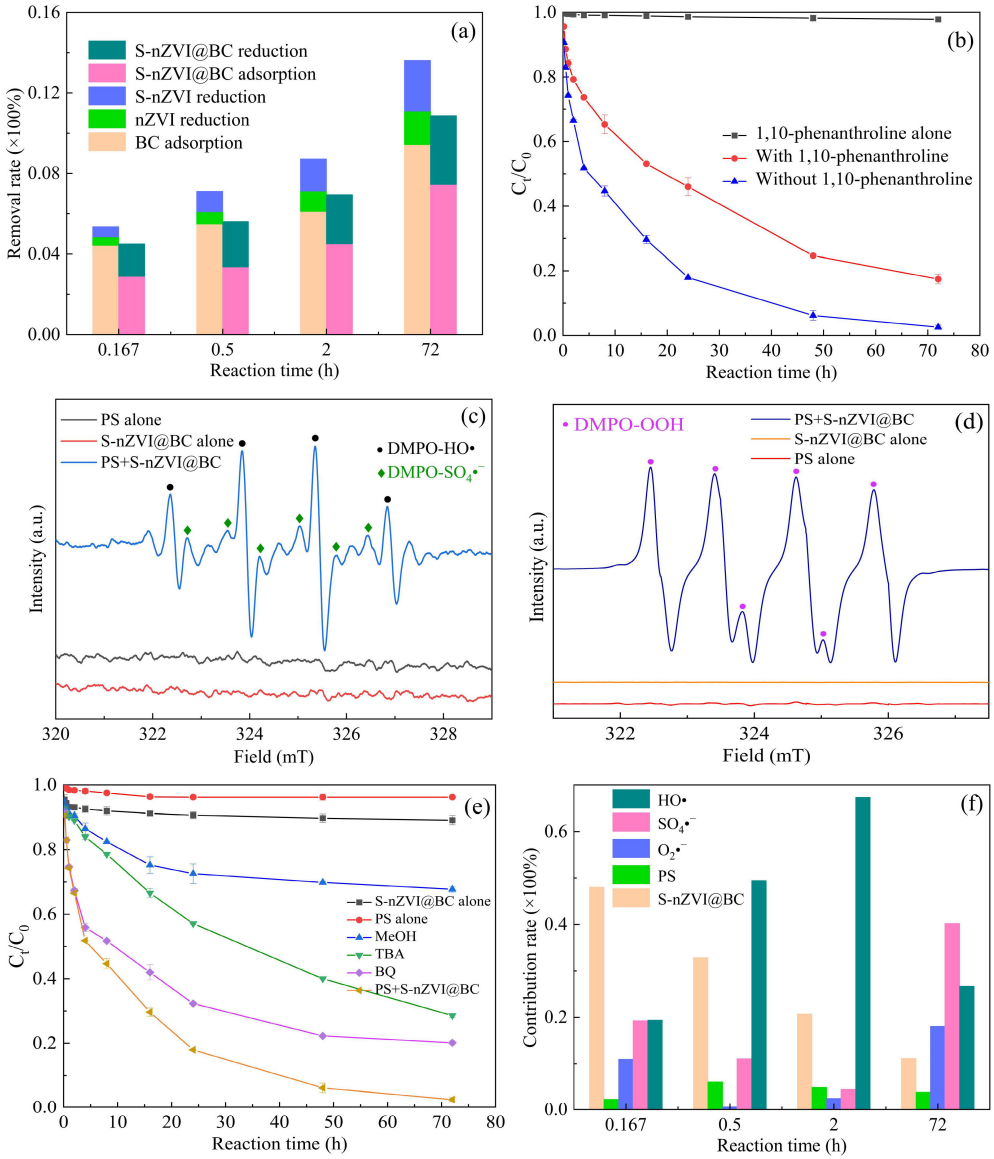


Figure 5. (**a**) Analysis of S-nZVI@BC ingredients' adsorption and reduction; (**b**) effect of 1,10-phenanthroline on inactivation of Fe^{2+}; (**c**) detection of HO• and SO_4•$^-$, (**d**) detection of O_2•$^-$; (**e**) removal of 2,4-DCP in different reaction systems; (**f**) contribution rates of five chemical factors at discrete time intervals. Reaction condition: PS = 1400 mg/L, [2,4-DCP] = 20 mg/L of 400 mL, BC@S-nZVI = 2100 mg/L, initial pH = 9 ± 0.2, T = 30 °C.

The persulfate activation mechanism in S-nZVI@BC/PS systems involves three iron species: (i) solid-phase Fe^0, (ii) dissolved Fe^{2+}, and (iii) surface-bound Fe^{2+}. To delineate their respective contributions, 1,10-phenanthroline (0.258 g, equimolar to theoretical iron content) was employed as a Fe^{2+} scavenger [45]. Figure 5b reveals the following: Control:

97.4% 2,4-DCP removal (72 h), Scavenger in solution: 82.5% removal (14.9% decrease), Scavenger alone: 2.2% removal (negligible adsorption). This demonstrates that Fe^0-mediated activation dominates (>80% contribution), while homogeneous/heterogeneous Fe^{2+} accounts for only 14.9% of the activation capacity. These findings align with Jin et al.'s report establishing solid Fe^0 as the primary PS activation pathway [32].

ESR spectroscopy with DMPO spin trapping was employed to identify reactive oxygen species (ROS) in the S-nZVI@BC/PS reaction system. As shown in Figure 5c, the characteristic signals of DMPO-HO• (1:2:2:1 quartet) and DMPO-SO_4•$^-$ were exclusively detected in the complete system, absent in PS-only and S-nZVI@BC-only controls. The attenuated DMPO-SO_4•$^-$ signal intensity is attributable to its transient nature and lower trapping efficiency [46]. Similarly, Figure 5d confirms O_2•$^-$ generation through DMPO-OOH adduct signatures [47]. These results collectively demonstrate the co-generation of HO•, SO_4•$^-$, and O_2•$^-$ radicals during 2,4-DCP degradation, consistent with the PS activation mechanisms reported for iron-based systems [36,48].

Radical quenching experiments were performed to quantify the contributions of key species (S-nZVI@BC, PS, HO•, SO_4•$^-$ and O_2•$^-$) to 2,4-DCP degradation. MeOH, TBA, and BQ served as scavengers for HO•/SO_4•$^-$, HO•, and O_2•$^-$, respectively, dosed at a 10:1 mass ratio relative to PS. Compared to the S-nZVI@BC/PS reaction system as shown in Figure 5e, the degradation efficiency at 72 h decreases from 97.4% to 10.9% in the presence of S-nZVI@BC alone, to 3.8% in the presence of PS alone, to 32.3% in the presence of MeOH, to 71.4% in the presence of TBA, and to 79.9% in the presence of BQ. Correspondingly, the contribution of various factors to the degradation of 2,4-DCP were different.

The relative contributions of five chemical factors were quantified by comparing 2,4-DCP removal efficiencies across experimental systems at discrete time intervals. Taking 72 h as a representative time point: the residual concentration ratio C_t/C_0 was 0.026 in the complete S-nZVI@BC/PS system, corresponding to 97.4% total removal. As the control systems showed, C_t/C_0 was 0.891 (10.9% removal) for S-nZVI@BC alone and 0.962 (3.8% removal) for PS alone. Radical quenching revealed partial contributions: C_t/C_0 was 0.677 with MeOH (SO_4•$^-$/HO• quenching) in the system, corresponding to 32.3% residual removal. C_t/C_0 was 0.286 with TBA (HO• quenching) in the system, corresponding to 71.4% residual removal. C_t/C_0 was 0.201 with BQ (O_2•$^-$ quenching) in the system, corresponding to 79.9% residual removal. Radical-specific contributions were derived by differential inhibition: SO_4•$^-$ contribution 39.1% (71.4–32.3%), HO• contribution 26.0% (97.4–71.4%), and O_2•$^-$ contribution 17.5% (97.4–79.9%). The final contribution rates were calculated by the ratio between 10.9%, 3.8%, 39.1%, 26.0%, and 17.5% to 97.4%, respectively, and the results were as follows: S-nZVI@BC 11.2%, PS 3.9%, SO_4•$^-$ 40.2%, HO• 26.7%, O_2•$^-$ 18.0%. The time-resolved contributions calculated analogously are summarized in Figure 5f.

The relative contribution of S-nZVI@BC (incorporating both adsorption and reductive dechlorination of 2,4-DCP) was highest (48.0%) at the initial reaction stage (0.167 h), which can be attributed to the abundant accessible sites on the BC surface. Subsequently, the contribution of HO• increased and exceeded other factors after 0.5 h, reaching a maximum of 67.3% at 2 h. This could be caused by the rapid activation of PS by Fe^0, favoring the generation of HO• (Equation (4)) over SO_4•$^-$ or O_2•$^-$ (Equations (3), (5) and (6)) at this stage. In the later reaction phase, the contribution of HO• declined, while that of SO_4•$^-$ became dominant (40.2% at 72 h), coinciding with the precipitation of $Fe(OH)_3$ resulting from OH^- consumption (Equation (11)). Meanwhile, the contribution of O_2•$^-$ stabilized at 18.1% after initial fluctuations.

3.6. Analysis of Degradation Pathway

The products of 2,4-DCP degradation were analyzed by an ultra high-resolution mass spectrometer, and the schematic pathways for 2,4-DCP degradation in the S-nZVI@BC/PS system are presented based on the obtained intermediates in Figure 6. The entire reaction was mainly divided into dechlorination, ring-opening, and mineralization. First, ortho-chloride on an aromatic ring of 2,4-DCP was directly reductive dechlorination by S-nZVI@BC, and the 4-chlorophenol (m/z = 127.16) was produced. Then, para-chloride on the intermediate product was further attacked and phenol (m/z = 93.03) was produced. Second, the aromatic ring was broken by ROS and PS, and low molecular weight products were generated, such as acetic acid (m/z = 60.95), propionic acid (undetected, predicted product based on Equation (16)), oxalic acid (m/z = 90.67), and maleic acid (undetected, predicted product based on Equation (17) [36]. Finally, the products with smaller molecular weights undergo further mineralization to CO_2 and H_2O. The biological toxicity intensities of the above several small-molecule organic substances in water are as follows: oxalic acid > maleic acid > propionic acid > acetic acid. However, their toxicity is much lower than that of 2,4-DCP at the low concentration condition.

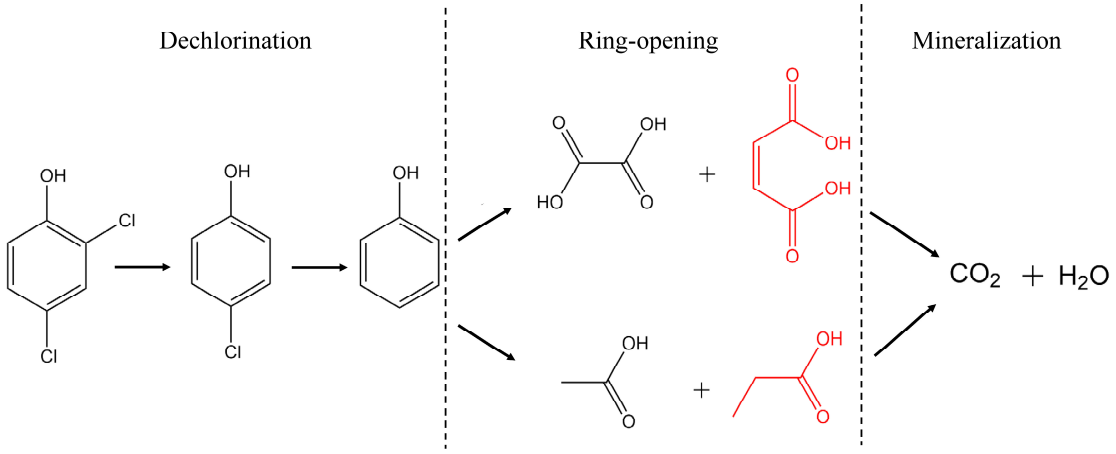


Figure 6. Degradation pathways of 2,4-DCP in the S-nZVI@BC/PS system. Reaction condition: PS = 1400 mg/L, [2,4-DCP] = 20 mg/L of 400 mL, BC@S-nZVI = 2100 mg/L, initial pH = 9 ± 0.2, T = 30 °C.

Furthermore, through total organic carbon (TOC) analysis, it was determined that the initial TOC of the 2,4-DCP solution was 8.7 mg/L, and it decreased to 2.1 mg/L after degradation for 72 h. This indicated that the TOC removal rate of the solution was 75.9%, while the removal rate of 2,4-DCP was 97.4% at this time. This confirmed that the 2,4-DCP degradation process involved the conversion into smaller organic compounds, and most of them were completely mineralized.

$$SO_4\bullet^- + HO\bullet + O_2\bullet^- + C_6H_6O \rightarrow SO_4^{2-} + C_3H_6O_2 + C_2H_4O_2 \quad (16)$$

$$SO_4\bullet^- + HO\bullet + O_2\bullet^- + C_6H_6O \rightarrow SO_4^{2-} + C_2H_2O_4 + C_4H_4O_4 \quad (17)$$

3.7. Summary and Reflection

Overall, comparing the findings of this article to the established literature, the results are summarized in Table 1. The basic research thoughts, analysis methods, and research results were consistent. However, this article focused more on the adsorption and reduction effects of S-nZVI@BC on 2,4-DCP, and conducted a detailed study on this. This article lacks electrochemical-related tests, and quantitative analysis electron transfer in a reaction system

is part of the study on the degradation mechanism. Meanwhile, the lack of quantifying PS generation to directly link catalyst activity to oxidant production is also a drawback of this article. The application of this system to real wastewater containing two or more contaminants is also worthy of deep research. These contents also represent the research directions in the near future.

Table 1. The finding comparisons of this research to the established literature.

Contents	This Research	The Established Literatures
To prepare S-nZVI@BC and characterize its microscopic shape	S-nZVI@BC was synthesized with two-step method in liquid phase; analyzed the microscopic structures, functional groups and chemical bonds of it	The preparation methods were mature, morphological characterization more comprehensive, and test equipment more advanced
To establish an S-nZVI@BC/PS reaction system for 2,4-DCP degradation	The optimal PS:2,4-DCP mass ratio was 70:1 and S-nZVI@BC:PS of 1.5:1; the degradation effect was better than that of either one or more components of the S-nZVI@BC/PS system	Due to the differences in material composition and degradable pollutants, the optimal ratios were not the same. However, the highest degradation rate of the entire system was consistent
To analyze different influencing factors of the system	The reusability of S-nZVI@BC, pH, temperature, and anions in solution was evaluated	The conventional influencing factors studied were the same
To quantify the contribution of S-nZVI@BC	Component contribution analysis quantified the adsorption and reduction in S-nZVI@BC; this was a notable highlight in this research	Some studies focused on the adsorption properties of S-nZVI@BC, but very little literature has paid attention to and quantitatively analyzed other chemical effects
To explore the PS activation mechanism	Fe^0 played a dominant role in the PS activation process, HO•, SO_4•$^-$, and O_2•$^-$ were key agents in subsequent degradation stages	The methods for determining the activation mode and identifying the active substances were basically the same
To analyze the degradation pathway	The degradation products and pathways were analyzed, but propionic acid and maleic acid were predicted products based on chemical equations	Every degradation product could be detected, and determined the clear degradation pathway

4. Conclusions

This study established an S-nZVI@BC-activating PS reaction system, and demonstrated exceptional 2,4-DCP degradation efficiency with varied influencing factors under the optimal conditions. The S-nZVI was stably loaded on the surface and in the pores of BC. The dominant activation was derived by Fe^0 in S-nZVI@BC, while adsorption predominated in the initial stage. Degradation proceeded via dechlorination, ring-opening, and mineralization, primarily mediated by HO•, SO_4•$^-$, and O_2•$^-$. In addition, the S-nZVI@BC had excellent stability and high reuse efficiency, the energy required for recycling it was lower than that needed for reproducing, and it also reduced the usage of related raw materials, leaded to high cost-effectiveness and sustainable usability. This work provides foundational insights for scaling up environmental remediation technologies, and will help advance the field of sustainability.

Supplementary Materials: The following supporting information can be downloaded at: https://www.mdpi.com/article/10.3390/su17198721/s1, Table S1: The total volume in pores and BET surface area statistics of materials; Figure S1: EDS images; Figure S2.: XPS analysis.

Author Contributions: Conceptualization, M.W. and C.D.; methodology, Y.Z. and Z.A.; software, M.W.; validation, M.W., Y.Z., Z.A. and C.D.; formal analysis, Z.A.; investigation, M.W. and Y.Z.; resources, Y.Z.; data curation, M.W.; writing—original draft preparation, M.W.; writing—review and editing, Y.Z.; visualization, M.W.; supervision, C.D.; project administration, Y.Z.; funding acquisition, C.D. All authors have read and agreed to the published version of the manuscript.

Funding: This research was funded by the Anhui Provincial Academy of Eco-Environmental Science Research grant number 52400198. And the APC was funded by the Anhui Provincial Academy of Eco-Environmental Science Research.

Institutional Review Board Statement: Not applicable.

Informed Consent Statement: Not applicable.

Data Availability Statement: The data are unavailable due to the related research topic still being under investigation.

Acknowledgments: This study is thankful for the support of Hefei Key Technology Major Research and Development Projects (2021GJ063) and National Natural Science Foundation of China for Young Scientists (52400198).

Conflicts of Interest: The authors declare no conflicts of interest.

References

1. Yadav, S.; Kumar, S.; Haritash, A.K. A comprehensive review of chlorophenols: Fate, toxicology and its treatment. *J. Environ. Manag.* **2023**, *342*, 118254. [CrossRef] [PubMed]
2. Yang, C.F.; Lee, C.M. Pentachlorophenol contaminated groundwater bioremediation using immobilized Sphingomonas cells inoculation in the bioreactor system. *J. Hazard. Mater.* **2008**, *152*, 159–165. [CrossRef]
3. Igbinosa, E.O.; Odjadjare, E.E.; Chigor, V.N.; Igbinosa, I.H.; Emoghene, A.O.; Ekhaise, F.O.; Igiehon, N.O.; Idemudia, O.G. Toxicological profile of chlorophenols and their derivatives in the environment: The public health perspective. *Sci. World J.* **2013**, *2013*, 460215. [CrossRef] [PubMed]
4. Zada, A.; Khan, M.; Khan, M.A.; Khan, Q.; Habibi-Yangjeh, A.; Dang, A.; Maqbool, M. Review on the hazardous applications and photodegradation mechanisms of chlorophenols over different photocatalysts. *Environ. Res.* **2021**, *195*, 110742. [CrossRef] [PubMed]
5. Li, R.C.; Jin, X.Y.; Megharaj, M.; Naidu, R.; Chen, Z.L. Heterogeneous Fenton oxidation of 2,4-dichlorophenol using iron-based nanoparticles and persulfate system. *Chem. Eng. J.* **2015**, *264*, 587–594. [CrossRef]
6. Garba, Z.N.; Zhou, W.M.; Lawan, I.; Xiao, W.; Zhang, M.; Wang, L.; Chen, L.; Yuan, Z. An overview of chlorophenols as contaminants and their removal from wastewater by adsorption: A review. *J. Environ. Manag.* **2019**, *241*, 59–75. [CrossRef]
7. Ma, T.G. Efficiency and Mechanism of Persulfate Activation by Polyaniline-Derived Carbon Materials for Chlorophenols Degradation in Water. Ph.D. Thesis, Jilin University, Changchun, China, November 2023.
8. Wang, J.L.; Chen, H. Catalytic ozonation for water and wastewater treatment: Recent advances and perspective. *Sci. Total Environ.* **2020**, *704*, 135249. [CrossRef]
9. Anjali, R.; Shanthakumar, S. Insights on the current status of occurrence and removal of antibiotics in wastewater by advanced oxidation processes. *J. Environ. Manag.* **2019**, *246*, 51–62. [CrossRef]
10. Zhou, Y.B.; Zhang, Y.L.; Hu, X.M. Enhanced activation of peroxymonosulfate using oxygen vacancy-enriched $FeCo_2O_{4-x}$ spinel for 2,4-dichlorophenol removal: Singlet oxygen-dominated nonradical process. *Colloids Surf. A* **2020**, *597*, 124568. [CrossRef]
11. Matzek, L.W.; Carter, K.E. Activated persulfate for organic chemical degradation: A review. *Chemosphere* **2016**, *151*, 178–188. [CrossRef]
12. Tsitonaki, A.; Petri, B.; Crimi, M.; Mosbaek, H.; Siegrist, R.L.; Bjerg, P.L. In situ chemical oxidation of contaminated soil and groundwater using persulfate: A review. *Crit. Rev. Environ. Sci. Technol.* **2010**, *40*, 55–91. [CrossRef]
13. Ike, I.A.; Linden, K.; Orbell, J.D.; Duke, M. Critical review of the science and sustainability of persulphate advanced oxidation processes. *Chem. Eng. J.* **2018**, *338*, 651–669. [CrossRef]
14. Wang, J.L.; Wang, S.Z. Reactive species in advanced oxidation processes: Formation, identification and reaction mechanism. *Chem. Eng. J.* **2020**, *401*, 126158. [CrossRef]
15. Ling, S.K.; Wang, S.; Peng, Y. Oxidative degradation of dyes in water using Co^{2+}/H_2O_2 and Co^{2+}/peroxymonosulfate. *J. Hazard. Mater.* **2010**, *178*, 385–389. [CrossRef] [PubMed]

16. Zhang, Y.Q.; Zhang, J.; Xiao, Y.; Chang, W.C.; Lim, T.T. Kinetic and mechanistic investigation of azathioprine degradation in water by UV, UV/H_2O_2 and UV/persulfate. *Chem. Eng. J.* **2016**, *302*, 526–534. [CrossRef]
17. Lee, J.; Von, G.U.; Kim, J.H. Persulfate-Based Advanced Oxidation: Critical Assessment of Opportunities and Roadblocks. *Environ. Sci. Technol.* **2020**, *54*, 3064–3081. [CrossRef] [PubMed]
18. Chen, G.Y.; Wu, G.Y.; Li, N.; Lu, X.K.; Zhao, J.H.; He, M.T.; Yan, B.B.; Zhang, H.Q.; Duan, X.G.; Wang, S.B. Landfill leachate treatment by persulphate related advanced oxidation technologies. *J. Hazard. Mater.* **2021**, *418*, 126355. [CrossRef]
19. Chen, H.; Zhang, Z.L.; Feng, M.B.; Liu, W.; Wang, W.; Yang, Q.; Hu, Y. Degradation of 2,4-dichlorophenoxyacetic acid in water by persulfate activated with FeS (mackinawite). *Chem. Eng. J.* **2017**, *313*, 498–507. [CrossRef]
20. Kim, C.L.; Ahn, J.Y.; Kim, T.Y.; Shin, W.S.; Hwang, I. Activation of Persulfate by Nanosized Zero-Valent Iron (NZVI): Mechanisms and Transformation Products of NZVI. *Environ. Sci. Technol.* **2018**, *52*, 3625–3633. [CrossRef]
21. Wang, S.S.; Zhao, M.Y.; Zhou, M.; Li, Y.C.; Wang, J.; Gao, B.; Sato, S.; Feng, K.; Yin, W.Q.; Igalavithana, A.D.; et al. Biochar-supported nZVI (nZVI/BC) for contaminant removal from soil and water: A critical review. *J. Hazard. Mater.* **2019**, *373*, 820–834. [CrossRef]
22. Jiang, X.Y.; Ouyang, Z.Z.; Zhang, Z.F.; Yang, C.; Li, X.Q.; Dang, Z.; Wu, P.X. Mechanism of glyphosate removal by biochar supported nano-zero-valent iron in aqueous solutions. *Colloids Surf. A* **2018**, *547*, 64–72. [CrossRef]
23. Cai, J.; Zhang, Y. Enhanced degradation of bisphenol S by persulfate activated with sulfide-modified nanoscale zero-valent iron. *Environ. Sci. Pollut. Res.* **2022**, *29*, 8281–8293. [CrossRef]
24. Wu, G.C.; Kong, W.J.; Gao, Y.; Kong, Y.; Dai, Z.G.; Dan, H.B.; Shang, Y.N.; Wang, S.Q.; Yin, F.J.; Yue, Q.Y.; et al. Removal of chloramphenicol by sulfide-modified nanoscale zero-valent iron activated persulfate: Performance, salt resistance, and reaction mechanisms. *Chemosphere* **2021**, *286*, 131876. [CrossRef] [PubMed]
25. Li, Y.F.; Hu, S.D.; Chen, J.H.; Muller, K.; Li, Y.C.; Fu, W.J.; Lin, Z.W.; Wang, H.L. Effects of biochar application in forest ecosystems on soil properties and greenhouse gas emissions: A review. *J. Soils Sediments* **2018**, *18*, 546–563. [CrossRef]
26. Xu, J.; Avellan, A.; Li, H.; Liu, X.T.; Noël, V.; Lou, Z.; Wang, Y.; Kaegi, R.; Henkelman, G.; Lowry, G.V. Sulfur Loading and Speciation Control the Hydrophobicity, Electron Transfer, Reactivity, and Selectivity of Sulfidized Nanoscale Zerovalent Iron. *Adv. Mater.* **2020**, *32*, e1906910. [CrossRef]
27. Chen, J.; Dong, H.R.; Tian, R.; Li, R.; Xie, Q.Q. Remediation of trichloroethylene-contaminated groundwater by sulfide-modified nanoscale zero-valent iron supported on biochar: Investigation of critical factors. *Water Air Soil Pollut.* **2020**, *231*, 432. [CrossRef]
28. Xie, R.H.; Wang, M.; Li, W.P.; Song, J.J. Degradation of 2-Chlorophenol in aqueous solutions using persulfate activated by biochar supported sulfide-modified nanoscale zero-valent iron: Performance and mechanisms. *Water* **2023**, *15*, 2805. [CrossRef]
29. Taiwo, K.J.; Oancea, A.V.; Kotha, N.S.; Usack, J.G. Enhancing wastewater treatment sustainability through integrated anaerobic digestion and hydrothermal carbonization: A life-cycle perspective. *Sustainability* **2025**, *17*, 7545. [CrossRef]
30. Kaynak, E.; Piri, I.S.; Das, O. Revisiting the Basics of Life Cycle Assessment and Lifecycle Thinking. *Sustainability* **2025**, *17*, 7444. [CrossRef]
31. Su, Y.M.; Jassby, D.; Song, S.K.; Zhou, X.F.; Zhao, H.Y.; Filip, J.; Petala, E.; Zhang, Y.L. Enhanced oxidative and adsorptive removal of diclofenac in heterogeneous Fenton-like reaction with sulfide modified nanoscale zerovalent iron. *Environ. Sci. Technol.* **2018**, *52*, 6466–6475. [CrossRef]
32. Jin, H.; Cang, Z.Z.; Ding, W.; Wu, W.T.; Ma, H.K.; Wang, C.X.; Qi, Z.W.; Li, Z.F.; Zhang, L.L. Oxidative removal of antibiotic resistant *E. coli* by sulfidated zero-valent iron: Homogeneous vs heterogeneous activation. *J. Hazard. Mater.* **2021**, *408*, 124411. [CrossRef]
33. Wang, X.Q.; Guo, Z.Z.; Hu, Z.; Ngo, H.H.; Liang, S.; Zhang, J. Adsorption of phenanthrene from aqueous solutions by biochar derived from anammoniation-hydrothermal method. *Sci. Total Environ.* **2020**, *733*, 139267. [CrossRef]
34. Zhao, H.Y.; Wang, Q.N.; Chen, Y.; Tian, Q.L.; Zhao, G.H. Efficient removal of dimethyl phthalate with activated iron-doped carbon aerogel through an integrated adsorption and electro-Fenton oxidation process. *Carbon* **2017**, *124*, 111–122. [CrossRef]
35. Zhang, P.; Song, D.; Xu, X.; Hao, Y.; Shang, X.; Wang, C.; Tang, J.; Sun, H. Sulfidated zero valent iron as a persulfate activator for oxidizing organo-phosphorus pesticides (OPPs) in aqueous solution and aged contaminated soil columns. *Chemosphere* **2021**, *281*, 130760. [CrossRef] [PubMed]
36. Wang, Y.Y.; Wang, L.; Zhang, Y.L.; Mao, X.H.; Tan, W.B.; Zhang, Y.L.; Wang, X.S.; Chang, M.; Guo, R.N.; Xi, B.D. Perdisulfate-assisted advanced oxidation of 2,4-dichlorophenol by bio-inspired iron encapsulated biochar catalyst. *J. Colloid Interface Sci.* **2021**, *592*, 358–370. [CrossRef] [PubMed]
37. Luo, X.W.; Shen, M.X.; Liu, J.H.; Ma, Y.J.; Gong, B.N.; Liu, H.Q.; Huang, Z.J. Resource utilization of piggery sludge to prepare recyclable magnetic biochar for highly efficient degradation of tetracycline through peroxymonosulfate activation. *J. Clean. Prod.* **2021**, *294*, 126372. [CrossRef]
38. Song, S.K.; Su, Y.M.; Adeleye, A.S.; Zhang, Y.L.; Zhou, X.F. Optimal design and characterization of sulfide-modified nanoscale zerovalent iron for diclofenac removal. *Appl. Catal. B-Environ.* **2017**, *201*, 211–220. [CrossRef]

39. Manz, K.E.; Carter, K.E. Investigating the effects of heat activated persulfate on the degradation of furfural, a component of hydraulic fracturing fluid chemical additives. *Chem. Eng. J.* **2017**, *327*, 1021–1032. [CrossRef]
40. Sun, Y.; Zhao, J.; Zhang, B.-T.; Li, J.; Shi, Y.; Zhang, Y. Oxidative degradation of chloroxylenol in aqueous solution by thermally activated persulfate: Kinetics, mechanisms and toxicities. *Chem. Eng. J.* **2019**, *368*, 553–563. [CrossRef]
41. Wang, Y.R.; Tian, D.F.; Chu, W.; Li, M.R.; Lu, X.W. Nanoscaled magnetic $CuFe_2O_4$ as an activator of peroxymonosulfate for the degradation of antibiotics norfloxacin. *Sep. Purif. Technol.* **2019**, *212*, 536–544. [CrossRef]
42. Gao, Y.Q.; Gao, N.Y.; Wang, W.; Kang, S.F.; Xu, J.H.; Xiang, H.M.; Yin, D.Q. Ultrasound-assisted heterogeneous activation of persulfate by nano zero-valent iron (nZVI) for the propranolol degradation in water. *Ultrason. Sonochem.* **2018**, *49*, 33–40. [CrossRef] [PubMed]
43. Wang, X.H.; Lin, Y.C. Phototransformation of cephalosporin antibiotics in an aqueous environment results in higher toxicity. *Environ. Sci. Technol.* **2012**, *46*, 12417–12426. [CrossRef] [PubMed]
44. Chen, J.S.; Luo, H.Y.; Luo, D.Y.; Chen, Y.; Tang, J.; Ma, H.; Pu, S.Y. New insights into the degradation of nitrobenzene by activated persulfate with sulfidated nanoscale zero-valent iron: Synergistic effects of reduction and reactive oxygen species oxidation. *Sep. Purif. Technol.* **2023**, *322*, 124252. [CrossRef]
45. Du, J.; Bao, J.; Lu, C.; Werner, D. Reductive sequestration of chromate by hierarchical FeS@Fe^0 particles. *Water Res.* **2016**, *102*, 73–81. [CrossRef]
46. Wang, Q.; Wang, B.B.; Ma, Y.; Xing, S.T. Enhanced superoxide radical production for ofloxacin removal via persulfate activation with Cu-Fe oxide. *Chem. Eng. J.* **2018**, *354*, 473–480. [CrossRef]
47. Webster, R.D. Electrochemistry combined with electron paramagnetic resonance (EPR) spectroscopy for studying catalytic and energy storage processes. *Curr. Opin. Electrochem.* **2023**, *40*, 101308. [CrossRef]
48. Liu, Y.; Zhao, Y.; Wang, J. Activation of peroxydisulfate by a novel Cu^0-Cu_2O@CNTs composite for 2, 4-dichlorophenol degradation. *Sci. Total Environ.* **2021**, *754*, 141883. [CrossRef]

Disclaimer/Publisher's Note: The statements, opinions and data contained in all publications are solely those of the individual author(s) and contributor(s) and not of MDPI and/or the editor(s). MDPI and/or the editor(s) disclaim responsibility for any injury to people or property resulting from any ideas, methods, instructions or products referred to in the content.